

Segmentation of Cardiac Cine MR Images for Extraction of Right and Left Ventricular Chambers

Ardeshir Goshtasby and David A. Turner

Abstract—A two-stage algorithm for extraction of the ventricular chambers (endocardial surfaces) in flow-enhanced magnetic resonance images is described. In the first stage, the approximate locations and sizes of the endocardial surfaces are determined by intensity thresholding. In the second stage, points on each approximated surface are repositioned to nearest locally maximum gradient magnitude points and a generalized cylinder is fitted to them. Examples of ventricular chambers in cine MR images determined by this algorithm are presented.

I. INTRODUCTION

DETERMINATION of cardiac function from magnetic resonance (MR) images requires determination of the volumes of the ventricular chambers at different phases of the cardiac cycle. In this paper, extraction of ventricular endocardial boundaries in 2-D images and ventricular endocardial surfaces in 3-D images are discussed. A two-stage algorithm is introduced which first determines the approximate positions and sizes of the ventricles using image intensities and then refines the ventricles using image edges. Segmentation of cardiac MR images is a difficult problem because intensities in such images depend on the blood velocity as well as on the tissue types [5], [21]. Although blood in the cardiac chambers appears as bright regions in flow-enhanced images, it does not have homogeneous intensities; as a result, the transition from the blood pool to surrounding myocardium is, at times, ambiguous.

Various methods for segmentation of cardiac MR images have been developed, many of which work on 2-D images. Extraction of endocardial ventricular boundaries by hand is simple but laborious and is subject to human operator bias [1], [15]. Various attempts to automate the segmentation process have been made. Bister *et al.* [2] designed a method which first segmented an image into regions of homogeneous intensities, and then based on some *a priori* knowledge, combined adjacent regions to construct the left ventricular chamber. Suh *et al.* [23] developed an expert system which

could use the zero-crossings of the second derivative of an image to locate the left ventricular boundary.

A semiautomatic method for determination of the left ventricular endocardial boundary is described by Wang *et al.* [26]. In this method, the user chooses a seed point on the endocardial boundary of the left ventricle. Then, based on the intensity gradient of the point and its neighbors, the next contour point is selected. The process is continued in this manner until either the seed point is reached or selection of the next contour point becomes ambiguous. In case of an ambiguity, control is passed to the user to manually draw the ambiguous segment, after which control is returned to the program to find the remainder of the contour. In another semiautomatic method described by Fleagle *et al.* [8], first, the user is asked to specify a point inside the left ventricular chamber. Then, by casting out radial lines from the selected point and applying an edge operator along the radial lines, a directed graph is constructed. Finally, the optimal path in the graph is searched and used as the left ventricular endocardial boundary.

A class of semiautomatic methods using energy minimizing curves is described by Cohen [4] and Kass *et al.* [16]. In these methods, a user draws the approximate boundary of a region of interest in an image. Then, an elastic curve is fitted to the boundary points and the curve is iteratively refined until its internal energy defined by its curvatures reaches the minimum while responding to external forces defined by image edges.

Three-dimensional methods for extraction of ventricular surfaces have also been developed. Most of these methods begin by segmenting a 3-D image slice by slice, either manually [22] or semiautomatically [19], and then by putting the segmented slices together construct the ventricular surfaces. A method that reconstructs the left ventricular surface from boundaries extracted in transverse, coronal, and sagittal slices of the heart has also been developed [6], [18].

A method that directly works on 3-D images is developed by Udupa [25]. In this method, first the image slices are interpolated into an isotropic volume data set, and then, by a semiautomatic procedure, the cardiac chambers are extracted. A method developed by Faber *et al.* [7] uses knowledge about the 3-D left ventricular shape to estimate the compatibility functions in a probabilistic relaxation labeling process. The process iteratively refines a given initial ventricular surface using the compatibility functions until either the process converges or the maximum allowed number of iterations is reached.

In the following, a two-stage algorithm for the extraction of ventricular endocardial boundaries in 2-D and ventricular

Manuscript received November 24, 1993; revised December 5, 1994. This work was partially supported by the American Heart Association of Metropolitan Chicago under Grant-In-Aid 2-5-38277. The Associate Editor responsible for coordinating the review of this paper and recommending its publication was E. McVeigh.

A. Goshtasby is with the Department of Electrical Engineering and Computer Science, University of Illinois at Chicago, Chicago, IL 60607-7053 USA; e-mail: ardeshir@eecs.uic.edu.

D. A. Turner is with the Department of Diagnostic Radiology and Nuclear Medicine, Rush-Presbyterian-St. Luke's Medical Center, Chicago, IL 60612 USA.

IEEE Log Number 9408770.

endocardial surfaces in 3-D images is described. Ventricular boundaries determined in 2-D images are represented by elastic curves, and ventricular endocardial surfaces obtained in 3-D images are represented by elastic surfaces. The uniqueness of this method is its ability to determine the curves and surfaces that represent the ventricular endocardial boundaries without any iterations or solution of a system of equations. It is based on a weighted averaging concept which determines the desired curves and surfaces by substituting the coordinates of given points into the provided equations. The elastic curves and surfaces allow high-resolution display of the ventricles and are suitable for animation of ventricular wall motion. The same steps are used to segment both 2-D and 3-D images. Section II discusses segmentation of 2-D MR slices, after which Section III presents segmentation of 3-D (volumetric) images.

II. SEGMENTATION OF MR SLICES

A. The Initial Segmentation

We have acquired cinematic magnetic resonance (cine MR) images (source images) with a 1.5-Telsa device (Signa: GE Medical Systems, Milwaukee). Imaging sections were 1 cm thick and contiguous; the matrix size was 256×256 , and the field of view was 31 cm. Cine MR images of the heart in each patient were acquired with software provided by the manufacturer [11].

Images were acquired in eight parallel planes, from the atrioventricular junction to the cardiac apex and perpendicular to the long axis of the left ventricle. Data were acquired from two image planes at the same time, so that the TR for each section (46 ms) was twice the data sampling time (23 ms). Thus, image data were acquired in all eight planes during a total of four acquisition periods. Two signals were averaged for each line of data. Since acquisition periods ranged from three to four minutes, depending on heart rate, the data collection periods lasted 12–16 min. The centers of the simultaneously acquired image levels were separated by 4 cm to minimize the adverse effects of blood saturation. TE was 12 ms, and the flip angle was 40° . The raw data were interpolated to construct 32 images through the “representative” cardiac cycle at each of the eight image levels, for a total of 256 images per study [11].

Blood that flows into the imaged volume during acquisition of images with this technique emits signals of higher intensity than tissue that remains in the volume during the entire acquisition, e.g., ventricular myocardium, a technique known as “flow enhancement.” Thus, the blood pools of the right and left ventricles appear as bright regions in the cine MR images. We use this information to determine the approximate positions of ventricular chambers.

The area covered by an MR image is known. By estimating the sizes of the ventricular chambers at a given cross-section and phase of the cardiac cycle, the fraction of the MR image covered by the chambers can be estimated. For example, the area covered by the image in Fig. 1(a) is $31 \text{ cm} \times 31 \text{ cm}$. This image shows the first MR slice in a sequence of eight short-axis cross-sections obtained from a patient at end-diastole. Computations from an average human heart have shown that

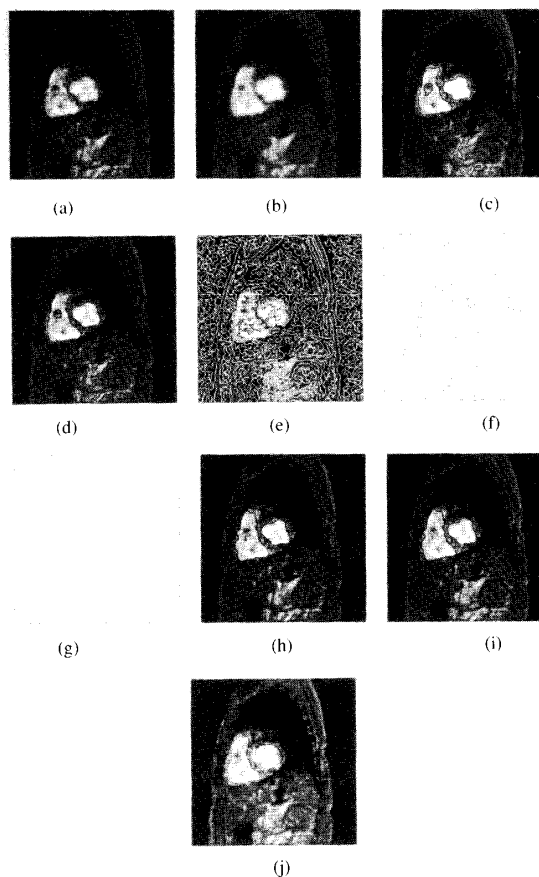


Fig. 1. (a) An MR source image near the base of the heart at end-diastole. (b) Smoothing of (a) with a Gaussian kernel of standard deviation two pixels. Regions obtained by classifying the (c) 4% and (d) 5% highest-intensity pixels in image (b) to the blood. (e) Zero-crossings of the Laplacian of Gaussian of image (a) using Gaussians of standard deviation two pixels. (f) Highest 20% gradient magnitude edges of (e). (g) Edge points in (f) that correspond to pixels in the initial ventricular endocardial boundaries obtained in (c). (h), (i) Final ventricular endocardial boundaries obtained when initial ventricular endocardial boundaries in (c) and (d), respectively, were used. (j) Manually traced ventricular boundaries of (a). These images show cross-sections of the ventricular chambers when viewed from the cardiac apex.

the area covered by the right and left ventricular chambers in a short-axis cross-section of the heart corresponding to this slice (the slice near the base of the heart) at end-diastole is about 40 cm^2 [22]. This area corresponds to about 4% of the entire MR slice in Fig. 1(a). Therefore, the MR source image was smoothed with a Gaussian kernel of standard deviation two pixels to reduce image noise (Fig. 1(b)), and the highest 4% intensities were classified to the blood to obtain the regions shown in Fig. 1(c).

The sizes of the ventricular chambers vary from one patient to another and the same 4% threshold cannot reliably extract the endocardial boundaries in all patients. Since information about shapes and sizes of ventricular chambers in a particular patient are usually not known, and some regions which do not represent the blood in the ventricular chambers could be obtained in this thresholding, the threshold of 4% can only act

as an approximation to true threshold value. If we segment the image in Fig. 1(b) by classifying the highest 5% intensities to the blood, we obtain the regions shown in Fig. 1(d). These regions are somewhat different from those found in Fig. 1(c). By examining Fig. 1(c) and (d) carefully, we see, however, that both images provide valuable information about the positions and shapes of the ventricles. The two largest regions in these images correspond to the ventricles. The proposed algorithm uses this information to estimate the initial shapes and positions of the ventricles. Then, it refines the ventricular regions using edge information in the image.

It is obvious that if initially selected regions do not correspond to the ventricular chambers, the final results will not show the chambers either. Slices near the apex of the heart contain ventricular regions that are small and may not represent the largest regions in an image. Therefore, segmentation is first carried out on the slice that is closest to the base of the heart, where ventricular regions are significantly larger than other regions. The centroids of the ventricular regions determined in the first slice are used to guide selection of regions in subsequent slices. Since the shapes of the ventricles can be represented by generalized cylinders and the long axis of the left ventricle is perpendicular to image slices in these images, the centroid of a ventricular cross-section in consecutive slices cannot displace by more than some threshold distance. By examining various image sequences, we have found that this displacement is never larger than eight pixels at this image resolution. Therefore, when regions corresponding to the ventricles in the i th slice are determined, a search is carried out in the $(i+1)$ st slice in windows of size 15×15 centered at the centroids of ventricles in the i th slice to determine the ventricular regions. Also, once the intensity threshold corresponding to the highest 4% intensities was determined in the first slice, the same intensity threshold is used to segment slices two through eight. This will ensure that the same range of intensities describe ventricular blood in all image slices.

The velocity of intraventricular blood varies not only during the cardiac cycle but also with its location within the ventricles. Since the brightness of blood varies with its flow velocity [21], variations in intensity are observed in the ventricular blood. Smoothing can be used to reduce intensity variations in the blood pools. Fig. 1(b) shows smoothing of Fig. 1(a) with a Gaussian filter of standard deviation two pixels. Larger Gaussian filters will further remove noise but, at the same time, will smooth out ventricular endocardial boundaries, and therefore are not recommended. As can be observed, the image after smoothing still shows the blood pools as the brightest regions. Therefore, intensity thresholding can be used to isolate them from the rest of the image. Our strategy will be to smooth a source image first, and then classify a given percentage of its highest intensities to the blood, and, in this manner, locate approximate positions of the ventricular chambers.

The sizes of the average normal left and right ventricular chambers are used as initial estimates of the sizes of the chambers in particular MR slices. Some error is tolerable in the initial segmentation, since the initial segmentation will be subsequently refined to find the final segmentation.

Although segmentation by intensity thresholding can approximately locate the ventricular chambers, it cannot accurately locate ventricular endocardial boundaries. Upon close inspection of the image intensities, we see that intensities across most sectors of the ventricular endocardial boundaries change sharply. This property will be used to refine the initial segmentation.

B. Region Boundaries from Locally Maximum Gradient Magnitudes

To separate regions of different intensities from each other in an image, we should search for image points whose gradient magnitudes are locally maximum. Locally maximum gradient magnitudes have previously been used in image segmentation [9], [14], [20]. Since points with locally maximum gradient magnitudes have second derivatives of zero, instead of computing locally maximum gradient magnitudes in an image, the zero-crossings of the second derivative of the image are used. Computation of image derivatives is, however, ill-conditioned in the presence of noise, and smoothing has been used to remedy this problem [24]. Therefore, smoothing of the source image was carried out by convolving the image with a Gaussian filter, and second derivatives were estimated by the Laplacian operator [20]. In implementation, these two operations were combined into a single, more efficient operation with the use of the Laplacian of Gaussian (LoG) mask to find the zero-crossings [20].

Fig. 1(e) shows the zero-crossings of the image in Fig. 1(a) obtained with the LoG operator of standard deviation two pixels. Many of the computed edges correspond to noisy intensity variations. These edges may be removed by examining the gradient magnitudes of the edges. Edges that have the highest 20% gradients in the image are shown in Fig. 1(f). Since gradient magnitudes at ventricular endocardial boundaries are usually high, keeping the highest 20% gradient magnitude edges will retain a sufficiently large number of pixels that include the ventricular boundaries. The remaining 80% of edges correspond to weaker intensity variations which have no role in determination of the ventricular endocardial boundaries and can be safely removed. The segmentation result is only slightly dependent on this threshold value. Retaining edges in Fig. 1(e) with the highest 15–40% gradients produced differences in segmentation results that were indistinguishable by the eye.

Ventricular endocardial boundary points are expected to exist among the edges detected by the LoG operator (Fig. 1(f)). However, ventricular boundaries determined in this manner may contain discontinuities. Moreover, some edges that do not belong to the ventricular endocardial boundaries are detected. To eliminate edges that do not belong to the ventricular boundaries, for each contour element on the ventricular endocardial boundaries obtained by intensity thresholding, the edge element closest to it is determined from among the obtained zero-crossing edges. This process, in effect, locally expands or shrinks the contours representing the ventricular boundaries in Fig. 1(c) in such a way that each contour element (pixel) will fall on an edge element in Fig. 1(f). Fig. 1(g) shows edge points obtained as a result of this processing. This step selects

zero-crossing edges that belong to the ventricular endocardial boundaries. The discontinuities in Fig. 1(g) show places where the ventricular boundaries in Fig. 1(c) had to be expanded to match edges in Fig. 1(f). A shrinkage corresponds to the mapping of two or more contour elements in Fig. 1(c) to the same edge element in Fig. 1(f). The edges selected in this manner could be noisy and disconnected. A process is required that will reduce noise and connect the edges to form closed ventricular boundaries. In the next section, a curve-fitting procedure is described which connects these edge elements and smooths noise between them to construct the ventricular boundaries.

C. Representing Ventricular Boundaries by Elastic Curves

A class of elastic curves known as rational Gaussian curves [12] will be used to describe the ventricular boundaries in this work. A rational Gaussian curve is defined by

$$\mathbf{P}(u) = \sum_{i=1}^n \mathbf{V}_i g_i(u) \quad u \in [0, 1] \quad (1)$$

where $\{\mathbf{V}_i: i = 1, \dots, n\}$ are the given points (points on a ventricular boundary as shown in Fig. 1(g)),

$$g_i(u) = \frac{W_i G_i(u)}{\sum_{j=1}^n W_j G_j(u)} \quad (2)$$

is the i th basis function of the curve, and

$$G_i(u) = \sum_{j=-J}^J \exp\{-[u - (u_i + j)]^2 / 2\sigma\}. \quad (3)$$

J is a small number ($0 \leq J \leq 5$) which depends on the accuracy of the computation and the standard deviation of the Gaussians [12]. Assuming required accuracy is ε and standard deviation of Gaussians used in curve fitting is σ , J is computed from [12]

$$J = \lceil \sigma \sqrt{-2 \ln \varepsilon} \rceil. \quad (4)$$

For instance, when $\sigma = 0.1$ and $\varepsilon = 10^{-8}$, we find $J = 1$. In the experiments reported in this paper, $J = 1$ was used. The standard deviation of Gaussians in (3) show the stiffness of the curve (decreasing the standard deviation will make the curve more elastic). W_i is the weight of the i th point and determines its degree of influence on the curve. We let the weight at a point be equal to its gradient magnitude so that a point with a larger gradient magnitude will have a larger influence on a generated curve.

Parameter u_i in (3) denotes the i th node of the curve. $\mathbf{P}(u_i)$ shows the point on the curve which receives the maximum influence from the i th edge point. An edge point affects an entire curve, however, and its effect decreases as one moves away from the corresponding node. The nodes of a curve determine the order in which the curve approximates the points. The points used in curve fitting in Fig. 1(g) were determined from points in the closed contours of Fig. 1(c). Since the order of points in the contours of Fig. 1(c) is known

and there is a one-to-one correspondence between points in the two images, the order of points in Fig. 1(g) becomes known. If points on a closed contour are labeled from 0 to $n-1$, u_i is simply i/n . u and σ should be measured with the same unit. For convenience, u was chosen to vary between zero and one to traverse an entire curve. Therefore, the ratio of the actual standard deviation of Gaussians used in an image to the number of pixels on a contour is used to represent the standard deviation of Gaussians in (3).

Fig. 1(h) shows rational Gaussian curves of standard deviation two pixels fitting the boundary pixels of Fig. 1(g). Increasing the standard deviation will make the obtained curves smoother. By removing small gradient magnitude edges from the image in Fig. 1(e) to obtain the image in Fig. 1(f), a considerable number of noisy edges have already been removed. For that reason, a small standard deviation, such as two pixels, is preferred over larger standard deviations in order that details in reconstructed ventricular boundaries are preserved and the boundaries are accurately positioned in an image.

If instead of Fig. 1(c), Fig. 1(d) was used as the initial segmentation, the result shown in Fig. 1(i) would be obtained. We see that, although the images in Fig. 1(c) and (d) are somewhat different, the images in Fig. 1(h) and (i) are almost the same. This demonstrates that some over- or underestimation of the ventricular sizes by intensity thresholding can be tolerated and the final segmentation is not very sensitive to the initial segmentation.

D. 2-D Segmentation Results

To evaluate the accuracy of the proposed image segmentation method, automatically obtained ventricular endocardial boundaries were compared with those determined by manual tracing. Earlier studies have demonstrated the reliability of manual tracing in determination of the ventricular boundaries in MR images [10], [17]. Ventricular boundaries of Fig. 1(a) manually traced by an experienced radiologist are shown in Fig. 1(j). Ventricular regions of the images in Fig. 1(h) and (j) were overlaid to determine their differences. To quantitate the differences, pixels in ventricular regions determined by the automatic and manual methods were set to 1 and other pixels in the images were set to 0. Then, exclusive-or of corresponding pixels in the images were determined. Segmentation error was defined as the ratio of the number of pixels with value 1 in the exclusive-ored image to the number of pixels with value 1 in the manually traced image. That is, if after setting pixels in the left ventricular regions in the images in Fig. 1(h) and (j) to 1 and setting all other pixels to 0, we obtain l_1 pixels with value 1 in the image in Fig. 1(j) and l_2 pixels with value 1 after exclusive-oring the images, then segmentation error for the left ventricle is defined by $E_l = l_2/l_1$. E_r is defined similarly using the right ventricular regions. Segmentation errors of image 1(h) defined in this manner were $E_l = 0.09$ and $E_r = 0.11$.

In the next experiment, the sequence of images shown in Fig. 2 was used. Each subimage shows one-fourth of a source image which covers the heart area. These images correspond to slices at end-diastole at eight levels through the ventricles. The boundary outlines were obtained using the proposed segmentation procedure with Gaussians of standard deviation

TABLE I
 ERRORS OF BOUNDARIES DETERMINED BY THE 2-D AUTOMATIC METHOD (FIG. 2), USING MANUALLY DETERMINED BOUNDARIES AS THE STANDARD OF REFERENCE

	Slice 1		Slice 2		Slice 3		Slice 4		Slice 5		Slice 6		Slice 7		Slice 8	
	E_l	E_r	E_l	E_r	E_l	E_r	E_l	E_r	E_l	E_r	E_l	E_r	E_l	E_r	E_l	E_r
Set 1	0.09	0.11	0.12	0.06	0.05	0.05	0.06	0.07	0.08	0.14	0.07	0.20	0.11	-	0.09	-
Set 2	-	-	0.05	0.10	0.07	0.09	0.12	0.08	0.11	0.11	0.09	0.10	0.15	0.12	0.12	0.20
Set 3	0.18	0.22	0.16	0.17	0.15	0.21	0.18	0.20	0.13	0.17	0.20	0.22	0.14	-	0.18	-
Set 4	0.12	0.20	0.08	0.18	0.13	0.07	0.08	0.08	0.06	0.12	0.09	0.16	0.15	-	0.20	-
Set 5	0.05	0.12	0.04	0.10	0.06	0.11	0.08	0.06	0.08	0.05	0.07	0.09	0.11	0.09	0.13	-

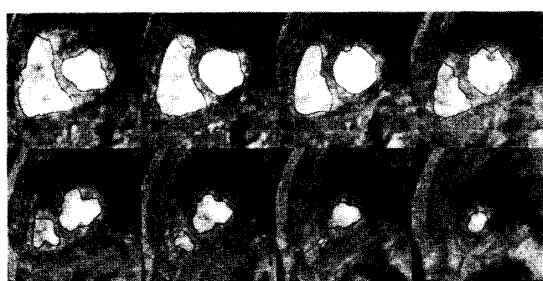


Fig. 2. A sequence of MR source images at end-diastole with obtained endocardial boundaries.

two pixels. Here, the highest 16% intensities in the image in Fig. 2(a) were classified as the blood. The highest 16%, rather than 4%, intensities were used because the area covered by Fig. 2(a) is one-fourth that of Fig. 1(a). The threshold value obtained in this manner was used to segment other image slices in Fig. 2 also. Note that this segmentation merely estimates the shapes and positions of ventricular endocardial boundaries. The shapes and positions of the obtained ventricular boundaries are refined using edge information in the images. To evaluate the segmentation results, manually traced ventricular boundaries were also determined. Segmentation errors were then computed and tabulated in the first row of Table I. Average errors for extraction of the left and right ventricular chambers were 0.08 and 0.10, respectively.

Entries in rows two through five of Table I show error measures on four more image sets. These images have been selected randomly from MR images routinely acquired in the Section of MRI at Rush-Presbyterian-St. Luke's Medical Center. Average errors for extraction of the left and right ventricular boundaries are 0.11 and 0.12, respectively. The first slice in the second data set contained parts of the atria and therefore was not used in the segmentation. The right ventricle did not exist in slices seven and eight in many of the image sets. Larger segmentation errors are obtained near the apex of the heart because extracted ventricular regions are small.

III. SEGMENTATION OF 3-D IMAGES

The procedure described for segmentation of 2-D images can be easily extended to 3-D. It is assumed that the given cross-sectional images are equally spaced. Since the resolution along the axis perpendicular to the slices in an MR set is

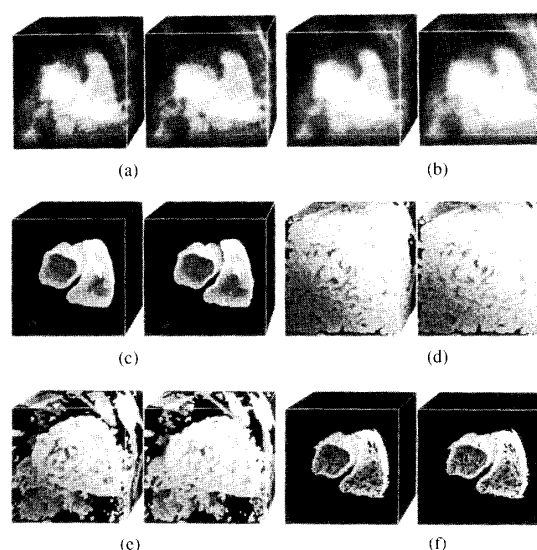


Fig. 3. (a) A volumetric cardiac MR image shown in stereo. (b) Image (a) after smoothing with a 3-D Gaussian kernel of standard deviation two pixels. (c) 3-D regions corresponding to the highest 9% intensities of image (b). (d) Zero-crossings of the second derivative of image (b). (e) Edges corresponding to the highest 20% gradient magnitudes of (d). (f) Edges of image (e) corresponding to voxels on the initial ventricular chambers shown in (c). These images show the ventricular chambers when viewed from the base of the heart. To view each stereo pair, hold a dark cardboard in such a way that one end of the cardboard separates the two images while its other end separates the two eyes. This will make each eye see only one image of the stereo pair and facilitate fusion of the images.

much lower than the resolution along the axis parallel to the slices, a procedure is required that transforms the slices into an isotropic 3-D array (volume image). An automatic procedure for this purpose has been developed and reported elsewhere [13]. Such a procedure is required to produce isotropic data so that when a 3-D Gaussian is used to smooth the slices, the Gaussian will smooth the image isotropically and not favor one direction against another. A volumetric image obtained from the given image slices is shown in stereo form in Fig. 3(a). This image pair was obtained by ray casting. To obtain each image, a ray was passed from a viewer's eye to each pixel on the screen and the average of intensities of image voxels intersecting the ray was computed and recorded at the screen pixel.

To smooth out small intensity variations inside the ventricular chambers, the volumetric image was convolved with a 3-D low-pass filter. Smoothing the image in Fig. 3(a) with a 3-D Gaussian of standard deviation two pixels, we obtain the image in Fig. 3(b). The image in Fig. 3(b) shows a block of size $15.5 \text{ cm} \times 15.5 \text{ cm} \times 8 \text{ cm}$ in 3-D. Knowing the volume of the ventricular chambers in an average healthy human heart at end-diastole, the percentage of such an image occupied by the chambers can be estimated. For instance, knowing that the average volume of the ventricular chambers at end-diastole in an average healthy heart is about 210 cm^3 [22], we estimate the chambers to occupy about 9% of the image shown in Fig. 3(b). Classifying voxels in the image in Fig. 3(b) whose intensities are among the highest 9% intensities to the blood, we obtain the segmentation result shown in Fig. 3(c). This image is shown in depth-map form: brighter points are closer to the viewer.

Ventricular endocardial surfaces extracted by intensity thresholding are not accurate, but rather, approximate the ventricular chambers. Locally maximum gradient magnitudes [3] are used to find the final ventricular endocardial surfaces. Locally maximum gradient magnitudes correspond to zero-crossings of the second derivative of an image. The zero-crossings of the second derivative of the image in Fig. 3(b) are shown in Fig. 3(d) in depth-map form. A large portion of the obtained zero-crossing edges correspond to weak and noisy intensity variations in the image which can be safely removed. Fig. 3(e) shows the zero-crossings of the second derivative of image in Fig. 3(b) whose gradient magnitudes are among the highest 20%. Gradient threshold values between 15% and 50% yielded segmentation results that were indistinguishable by the eye.

The ventricular chambers are hidden among the extracted edges in Fig. 3(e). To determine the points that belong to ventricular endocardial surfaces, a procedure similar to that developed for 2-D images is followed. For each voxel on a ventricular endocardial surface obtained by intensity thresholding, the edge point closest to it is determined from among the zero-crossing edges. This process, in effect, locally expands or shrinks the initial ventricular surfaces in such a way that each surface element in Fig. 3(c) reaches an edge element in Fig. 3(e). In our experiment, this process produced the edge elements shown in Fig. 3(f). The holes in the surfaces show places where expansion has occurred when deforming the endocardial surfaces in Fig. 3(c) to conform to edges detected in Fig. 3(e). Voxels in Fig. 3(f) are used in a surface fitting process to reconstruct the ventricular surfaces.

Ventricular endocardial surfaces have the shape of a generalized cylinder. The cross-sections of a generalized cylinder vary in shape and size as one moves along the axis of the cylinder, but their topologies remain the same. If an elastic generalized cylinder is fitted to edge points on each ventricular surface of Fig. 3(f), the generalized cylinders will connect the points and smooth out noise among them.

An elastic generalized cylinder is defined by [12]

$$\mathbf{P}(u, v) = \sum_{i=1}^n \mathbf{V}_i g_i(u, v), \quad u, v \in [0, 1], \quad (5)$$

where n is the number of given points, \mathbf{V}_i is the coordinates of the i th edge point,

$$g_i(u, v) = \frac{W_i G_i(u, v)}{\sum_{j=1}^n W_j G_j(u, v)} \quad (6)$$

is the i th basis function of the surface, and

$$G_i(u, v) = \sum_{j=-J}^J \exp(-\{[u - (u_i + j)]^2 + (v - v_i)^2\}/\sigma^2). \quad (7)$$

If we keep parameter v fixed and vary parameter u , $\mathbf{P}(u, v)$ will trace a short-axis cross-section of the generalized cylinder; whereas, if we keep u fixed and vary v , $\mathbf{P}(u, v)$ will trace a curve on the cylinder along its long axis. The standard deviation of Gaussians control the elasticity of the generated surface. The smaller the standard deviation, the more elastic the surfaces and thus, the more detailed and localized the ventricular surfaces. The larger the standard deviations, the smoother the obtained surfaces.

(u_i, v_i) is the i th node of the surface and determines the adjacency relation between point \mathbf{V}_i and neighboring points. u_i shows the order of \mathbf{V}_i in the closed contour of the image slice where it appeared, and can be determined in the same manner as the nodes of a curve (see Section II-C). v_i is proportional to the slice number of \mathbf{V}_i . If there are $m+1$ slices labeled from 0 to m , and if point \mathbf{V}_i belongs to the j th slice, then $v_i = j/m$. Parameter J in (7) depends on the accuracy of the computation and is computed from (4) [12]. In this paper, $J = 1$ was used.

Fig. 4(a) and (b) shows different views of generalized cylinders of standard deviation two pixels fitting the edges of Fig. 3(f). Shown here are ventricular chambers viewed from the base of the heart toward the cardiac apex (Fig. 4(a)) and from the left posterior toward the right anterior of the heart (Fig. 4(b)). Repeating the same process using standard deviation of Gaussians equal to three pixels in both the zero-crossing operation and the surface fitting process, we obtain the surfaces shown in Fig. 4(c) and (d). As the standard deviation of Gaussians increases, smoother surfaces are obtained. Too large a standard deviation, however, will smooth out critical details on the ventricular surfaces and should be avoided. Since edges corresponding to the lowest 80% of image gradients have been removed from the zero-crossing edges, a large proportion of noisy edges have already been removed from the images, and a small standard deviation, such as two pixels, is sufficient to localize the ventricles and preserve anatomic details.

To evaluate the segmentation results, cross-sections of the constructed generalized cylinders at the original slices (Fig. 2) were obtained and shown in Fig. 5. The difference between corresponding slices in Figs. 2 and 5 arise from the fact that a slice in Fig. 2 was segmented independently of other slices, while all of the slices in Fig. 5 interacted with each other

TABLE II
 ERRORS OF BOUNDARIES DETERMINED BY THE 3-D AUTOMATIC METHOD (FIG. 5), USING MANUALLY DETERMINED BOUNDARIES AS THE STANDARD OF REFERENCE

	Slice 1		Slice 2		Slice 3		Slice 4		Slice 5		Slice 6		Slice 7		Slice 8	
	E_l	E_r	E_l	E_r	E_l	E_r	E_l	E_r	E_l	E_r	E_l	E_r	E_l	E_r	E_l	E_r
Set 1	0.07	0.08	0.07	0.04	0.03	0.05	0.03	0.06	0.07	0.06	0.05	0.05	0.07	-	0.06	-
Set 2	-	-	0.05	0.07	0.05	0.06	0.05	0.04	0.07	0.08	0.05	0.09	0.08	0.08	0.04	0.14
Set 3	0.06	0.12	0.11	0.09	0.07	0.10	0.07	0.12	0.12	0.15	0.08	0.15	0.12	-	0.11	-
Set 4	0.07	0.08	0.07	0.11	0.08	0.05	0.03	0.04	0.05	0.07	0.09	0.08	0.06	-	0.12	-
Set 5	0.05	0.09	0.05	0.08	0.05	0.07	0.04	0.04	0.06	0.04	0.05	0.06	0.07	0.04	0.10	-

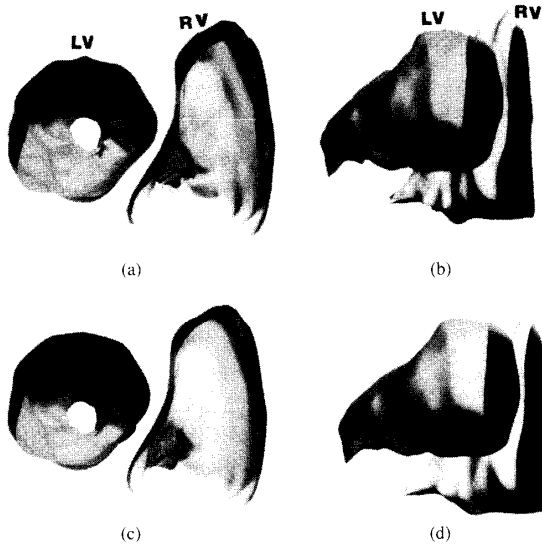


Fig. 4. (a), (b) Ventricular endocardial surfaces obtained by fitting rational Gaussian surfaces of standard deviation two pixels to points on ventricular chambers shown in Fig. 3(f). The ventricles are viewed (a) from the base toward the cardiac apex and (b) from the left posterior toward the right anterior of the heart. (c), (d) Ventricular endocardial surfaces obtained when standard deviations of Gaussians used in image smoothing and surface fitting were increased to three pixels.

to produce the segmentation result. This interaction smooths sharp differences in segmentation results between adjacent slices.

The first row of Table II compares segmentation errors of the automatic method (Fig. 5) against the manual method, using the manual method as the standard. By comparing these results with those shown in Table I, we see that the 3-D method has produced considerably lower errors than the 2-D method. Average segmentation errors for the left and right ventricles by the 3-D method are 0.06 and 0.07, respectively.

Computationally, the proposed segmentation method takes three minutes to transform eight short-axis cardiac images of size 128×128 into an isotropic $128 \times 128 \times 57$ volume image, eleven minutes to determine the 3-D zero-crossing edges from the volume image, and two minutes to fit two elastic generalized cylinders to the obtained edges on a Sun SparcStation II computer. Total computation time for

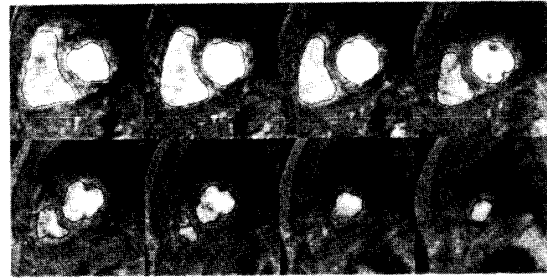


Fig. 5. Cross-sections of ventricular endocardial surfaces of Fig. 4(a) at slices corresponding to those shown in Fig. 2.

extraction of ventricular boundaries in 2-D images of size 128×128 is about one minute.

IV. DISCUSSION AND CONCLUSIONS

Since the heart moves parallel to its long axis during a cardiac cycle, a short-axis image at different phases of the cardiac cycle does not always contain the same cross-section of the heart. For that reason, measurement of local cardiac function, such as assessment of regional wall motion or wall thickening from segmentation of image slices, is inherently inaccurate. Since the entire heart during motion remains in a fixed 3-D window defined by the field of view of the MR scanner, segmentation of volumetric images potentially can yield more accurate measurements of local myocardial function. In addition, information shared between image slices in the 3-D method reduces segmentation error due to noise within slices.

In the proposed image segmentation method, the initial segmentation obtained by intensity thresholding defines the topology of the ventricular chambers and the zero-crossings of the second derivative of an image determine the final segmentation result. The points used in curve or surface fitting are selected from the zero-crossing edges and are weighted by their gradient magnitudes. The objective in curve or surface fitting is to reduce the effect of falsely detected boundary or surface points and make the final boundaries or surfaces pass closer to points with larger gradient magnitudes which are more likely to represent the ventricular endocardial boundaries or surfaces.

The choice of the standard deviations of Gaussians used in image smoothing and curve and surface fitting affect the final segmentation result. If a very wide Gaussian smoothing is used, the left and right ventricles may merge into one. On the other hand, if a very narrow Gaussian smoothing is used, signal variations inside a ventricular chamber may break the chamber into two or more regions. Since region topologies determined by intensity thresholding are used to guide the segmentation, it is important that the thresholding process detects two regions that approximately represent the ventricles. In experiments with clinical MR images of the heart, we have found that standard deviation of Gaussians about two pixels produces the most desirable segmentation results.

The standard deviation of Gaussians used in curve and surface fitting controls the elasticity of obtained curves and surfaces. The smaller the standard deviation of Gaussians, the more elastic the obtained curves and surfaces, resulting in better reconstruction of image details. As the standard deviation of Gaussians increases, the curves and surfaces become less elastic and tend to smooth details in ventricular boundaries or surfaces. We have chosen the standard deviation of Gaussians used in image smoothing to be the same as the standard deviation of Gaussians used in curve and surface fitting. This is done because when a smaller standard deviation Gaussian smoother is used, more detailed ventricular boundaries will be obtained and, to preserve the obtained details, curves and surfaces with larger elasticities (smaller standard deviations) should be used. On the other hand, when a larger standard deviation of Gaussian smoother is used, less detailed ventricular boundaries will be obtained, requiring curves and surfaces with smaller elasticities (larger standard deviations) to reconstruct them.

Ventricular endocardial surfaces obtained by the proposed method are in analytic form, enabling direct computation of the surface normals for display purposes. Fig. 4(a)–(d) was generated from the analytic surface normals. This is in contrast to methods whose final results are in digital form and require a computationally intensive procedure to fit polynomial patches to local data to determine the surface normals.

The proposed method cannot extract the epicardial surfaces from MR images because portions of the heart walls and surrounding tissues have similar intensities, and the thresholding step which should determine the topology of the epicardial surface fails. We are planning to use a model of the human heart to aid extraction of the epicardial surfaces.

For the method to work automatically without any user interaction, the provided images should not contain the atria. Also, the images must be flow-enhanced so that pixel (voxel) averages in small neighborhoods in the blood pools are higher than pixel (voxel) averages representing the surrounding tissues.

In summary, a novel method for segmentation of 2-D and 3-D cardiac MR images was introduced which first estimates the locations of the ventricles by intensity thresholding and then repositions points on ventricular endocardial boundaries and surfaces to nearest points with locally maximum gradient magnitudes. The refined points are then used in a curve or surface fitting process to determine the boundaries or surfaces

of the ventricular chambers. Some of the characteristics of the proposed segmentation method are:

- 1) It requires no user interaction.
- 2) It can segment volumetric MR images and extract the endocardial surfaces of the ventricular chambers.
- 3) Extracted ventricular endocardial surfaces are in analytic form, lending themselves to high resolution display and animation of ventricular wall motion.
- 4) Ventricular endocardial surfaces are represented by elastic surfaces whose degrees of elasticity can be varied to control the smoothness of the reconstructed endocardial surfaces.

ACKNOWLEDGMENT

We are thankful to the reviewers and Dr. M. Belohlavek, Division of Cardiovascular Diseases and Internal Medicine, Mayo Clinic for their insightful comments and suggestions.

REFERENCES

- [1] E. L. Alderman, H. Sadler, J. Z. Brooker, W. J. Sanders, C. Simpson, and D. C. Harrison, "Light-pen computer processing of video images for the determination of left ventricular volume," *Circ.*, vol. 47, pp. 309–316, Feb. 1973.
- [2] M. Bister, Y. Taeymans, and J. Cornelis, "Automated segmentation of cardiac MR images," *Proc. IEEE Comput. Cardiol.*, pp. 215–218, 1989.
- [3] M. Bomans, K.-H. Hohne, U. Tiede, and M. Riemer, "3-D segmentation of MRI images of the head for 3-D display," *IEEE Trans. Med. Imag.*, vol. 9, pp. 177–183, 1990.
- [4] L. D. Cohen, "On active contour models and balloons," *Image Understanding*, vol. 53, no. 2, pp. 211–218, 1991.
- [5] P. L. Davis, L. Kaufman, and L. Crooks, "Tissue characterization," in *Clinical Magnetic Resonance Imaging*, A. R. Margulis, C. B. Higgins, L. Kaufman, and L. E. Crooks, Eds. Radiology Research and Education Foundation, 1983, pp. 53–77.
- [6] S. Eihō and A. Amano, "3-D reconstruction of myocardium from MRI and a display system of pulsating 3-D heart image," *Proc. IEEE Comput. Cardiol.*, pp. 211–214, 1989.
- [7] T. L. Faber, E. M. Stokely, R. M. Peshock, and J. R. Corbett, "A model-based four-dimensional left ventricular surface detector," *IEEE Trans. Med. Imag.*, vol. 10, no. 3, pp. 321–329, 1991.
- [8] S. R. Fleagle, D. R. Thedens, J. C. Ehrhardt, T. D. Scholz, and D. J. Skorton, "Automated identification of left ventricular borders from spin-echo magnetic resonance images," *Invest. Radiol.*, vol. 26, no. 4, pp. 295–303, 1991.
- [9] M. M. Fleck, "Some defects in finite difference edge finders," *IEEE Trans. Pattern Anal. Mach. Intell.*, vol. 14, no. 3, pp. 337–345, 1992.
- [10] M. S. Florentine, C. L. Grosskreutz, W. Chang, J. A. Hartnett, V. D. Dunn, J. C. Ehrhardt, S. R. Fleagle, S. M. Collins, M. L. Marcus, and D. J. Skorton, "Measurement of left ventricular mass *in vivo* using gated nuclear magnetic resonance imaging," *J. Amer. Coll. Cardiol.*, vol. 8, no. 1, pp. 107–112, 1986.
- [11] G. H. Glover and N. J. Pelc, "A rapid-gated cine MRI technique," in *Magnetic Resonance Annual*, H. Y. Kressel, Ed. New York: Raven Press, 1988, pp. 299–333.
- [12] A. Goshtasby, "Design and recovery of 2-D and 3-D shapes using rational Gaussian curves and surfaces," *Int. J. Comput. Vision*, vol. 10, no. 3, pp. 233–256, 1993.
- [13] A. Goshtasby, D. A. Turner, and L. V. Ackerman, "Matching of tomographic slices for interpolation," *IEEE Trans. Med. Imag.*, vol. 11, no. 4, pp. 507–516, 1992.
- [14] R. M. Haralick, "Digital step edges from zero-crossings of second directional derivatives," *IEEE Trans. Pattern Anal. Mach. Intell.*, vol. PAMI-6, no. 1, pp. 58–68, 1984.
- [15] P. H. Heintzen, V. Malerczyk, and K. W. Scheel, "Online processing of the video image for left ventricular volume determination," *Comput. Biomed. Res.*, vol. 4, pp. 474–485, 1971.
- [16] M. Kass, A. Witkin, and D. Terzopoulos, "Snakes: Active contour models," *Int. J. Comput. Vision*, vol. 1, pp. 321–331, 1987.
- [17] A. M. Keller, R. M. Peshock, C. R. Malloy, L. M. Bujar, R. Nunnally, R. W. Parkey, and J. T. Willerson, "In vivo measurement of myocar-

- dial mass using nuclear magnetic resonance imaging," *J. Amer. Coll. Cardiol.*, vol. 8, no. 1, pp. 113–117, 1986.
- [18] M. Kuwahara and S. Eiho, "3-D heart image reconstruction from MRI data," *Comput. Med. Imag. Graphics*, vol. 15, no. 4, pp. 241–246, 1991.
- [19] W. Markiewicz, U. Sechtem, R. Kirby, N. Derugin, G. C. Caputo, and C. B. Higgins, "Measurement of ventricular volumes in the dog by nuclear magnetic resonance imaging," *J. Amer. Coll. Cardiol.*, vol. 10, no. 1, pp. 170–177, 1987.
- [20] D. Marr and E. C. Hildreth, "Theory of edge detection," *Proc. Royal Soc. London*, vol. B-207, pp. 187–217, 1980.
- [21] G. K. von Schutthess, "The effects of motion and flow on magnetic resonance imaging," in *Morphology and Function in MRI*. New York: Springer-Verlag, 1989, ch. 3, pp. 43–62.
- [22] U. Sechtem, P. W. Pflugfelder, R. G. Gould, M. M. Cassidy, and C. B. Higgins, "Measurement of right and left ventricular volumes in healthy individuals with cine MR imaging," *Radiology*, vol. 163, no. 3, pp. 697–702, 1987.
- [23] D. Y. Suh, R. L. Eisner, R. M. Mersereau, and R. I. Pettigrew, "Knowledge-based system for boundary detection of four-dimensional cardiac magnetic resonance image sequences," *IEEE Trans. Med. Imag.*, vol. 12, no. 1, pp. 65–72, 1993.
- [24] V. Torre and T. A. Poggio, "On edge detection," *IEEE Trans. Pattern Anal. Mach. Intell.*, vol. PAMI-8, pp. 146–163, Mar. 1986.
- [25] J. K. Udupa, "Interactive segmentation and boundary surface formation for 3-D digital images," *Comput. Graphics Image Process.*, vol. 18, pp. 213–235, 1982.
- [26] J. Z. Wang, D. A. Turner, and M. D. Chutuape, "Fast, interactive algorithm for segmentation of a series of related images: Application to volumetric analysis of MR images of the heart," *J. Magnet. Reson. Imag.*, vol. 2, no. 5, pp. 575–582, 1992.